HHS Public Access

Author manuscript

Magn Reson Med. Author manuscript; available in PMC 2018 July 01.

Published in final edited form as:

Magn Reson Med. 2017 July ; 78(1): 264–270. doi:10.1002/mrm.26358.

MRI-based quantitative susceptibility mapping (QSM) and R2* mapping of liver iron overload: comparison with SQUID-based biomagnetic liver susceptometry

Samir D. Sharma[1,*], **Roland Fischer**[2,3], **Bjoern P. Schoennagel**[4], **Peter Nielsen**[2,5], **Hendrik Kooijman**[6], **Jin Yamamura**[4], **Gerhard Adam**[4], **Peter Bannas**[1,4], **Diego Hernando**[1], and **Scott B. Reeder**[1,7,8,9,10]

[1]Department of Radiology, University of Wisconsin, Madison, Wisconsin, USA

[2]Department of Pediatric Hematology/Oncology, University Medical Center Hamburg-Eppendorf, Hamburg, Germany

[3]UCSF Benioff Children's Hospital and Research Center Oakland, Oakland, California, USA

[4]Department of Diagnostic and Interventional Radiology, University Medical Center Hamburg-Eppendorf, Hamburg, Germany

[5]Department of Biochemistry and Molecular Cell Biology, University Medical Center Hamburg-Eppendorf, Hamburg, Germany

[6]Philips GmbH, Hamburg, Germany

[7]Department of Medical Physics, University of Wisconsin, Madison, Wisconsin, USA

[8]Department of Biomedical Engineering, University of Wisconsin, Madison, Wisconsin, USA

[9]Department of Medicine, University of Wisconsin, Madison, Wisconsin, USA

[10]Department of Emergency Medicine, University of Wisconsin, Madison, Wisconsin, USA

Abstract

Purpose—We aimed to determine the agreement between quantitative susceptibility mapping (QSM)-based biomagnetic liver susceptometry (BLS) and confounder-corrected R2* mapping with superconducting quantum interference device (SQUID)-based biomagnetic liver susceptometry in patients with liver iron overload.

Methods—Data were acquired from two healthy controls and 22 patients undergoing MRI and SQUID-BLS as part of routine monitoring for iron overload. MR imaging was performed on a 3T system using a 3D multi-echo, gradient-echo acquisition. Both magnetic susceptibility and R2* of the liver were estimated from this acquisition. Linear regression was used to compare estimates of QSM-BLS and R2* to SQUID-BLS.

Results—Both QSM-BLS and confounder-corrected R2* were sensitive to the presence of iron in the liver. Linear regression between QSM-BLS and SQUID-BLS demonstrated the following

[*]Correspondence to: Samir D. Sharma, Ph.D., Department of Radiology, University of Wisconsin, WIMR2 #2480, 1111 Highland Ave., Madison WI 53705, sdsharma2@wisc.edu.

relationship: QSM-BLS = (−0.22 ± 0.11) + (0.49 ± 0.05) · SQUID-BLS with $r^2 = 0.88$. The coefficient of determination between liver R2* and SQUID-BLS was also $r^2 = 0.88$.

Conclusion—We determined a strong correlation between both QSM-BLS and confounder-corrected R2* to SQUID-BLS. This study demonstrates the feasibility of QSM-BLS and confounder-corrected R2* for assessing liver iron overload, particularly when SQUID systems are not accessible.

Keywords

magnetic susceptibility; quantitative susceptibility mapping; liver iron overload; R2* mapping; SQUID

INTRODUCTION

Excessive accumulation of iron in the body is toxic and can lead to multiple health complications including liver and heart damage, pancreatic dysfunction, and growth failure through pituitary dysfunction. The body has very limited natural capabilities to remove excess iron, therefore phlebotomy or chelation treatment is often prescribed for patients with iron overload (1). Chelation therapy is effective at removing excess iron from the body, however it is also expensive, can be difficult to ensure proper dosing, and introduces its own side effects (2,3). Therefore, the ability to routinely monitor body iron concentration is essential for ensuring proper dose adjustment of chelation therapy while also minimizing the potential for adverse side effects.

Serum markers, most commonly ferritin, are often used to assess body iron concentration. While simple and inexpensive, ferritin can be confounded by a number of factors including inflammation. The presence of confounding factors limits the accuracy of serum markers for assessing body iron concentration (4).

Liver iron concentration (LIC) is a reliable indicator of body iron concentration (5). Measurement of LIC can be performed using a liver biopsy. Biopsy can accurately measure LIC, however it is invasive, painful, and suffers from high sampling variability (6). Furthermore, biopsy is contraindicated in patients with thrombocytopenia or bleeding diatheses due to the risk of uncontrolled bleeding. In regular iron monitoring of patients, it is not desirable to perform biopsies on an annual or biennial timeline. Therefore, non-invasive techniques for assessing LIC are needed.

Biomagnetic liver susceptometry (BLS) using a superconducting quantum interference device (SQUID) is the current noninvasive reference standard for measurement of LIC (7–9). An advantage of SQUID-BLS is that it measures magnetic susceptibility, which is a quantitative property of tissue. The presence of iron significantly alters the magnetic susceptibility of the liver, which can be measured to determine the LIC. Despite the advantages of SQUID-BLS, the lack of access to a SQUID biomagnetometer for measurement of liver susceptibility (only four systems worldwide) has limited the widespread adoption of this technique.

MRI is a widely available technology that, like SQUID, is exquisitely sensitive to the magnetic susceptibility of tissue. The tissue susceptibility distorts the main magnetic (i.e. B0) field, which can be measured using a gradient-echo acquisition. MRI-based quantitative susceptibility mapping (QSM) techniques have been developed and validated over recent years (10–12). QSM has primarily focused on applications in the brain, to distinguish calcification from hemosiderin (13,14), to quantify iron concentration in deep brain regions (15,16), as well as to measure the biodistribution of paramagnetic contrast agents in perfusion imaging (17,18).

Recently, a QSM technique for the abdomen was developed and its feasibility was demonstrated in patients with liver iron overload (19). This technique addresses the challenges of QSM outside of the brain, including the presence of fat, physiological motion during the acquisition, as well as the potential for large susceptibility shifts, which increases R2* signal decay. QSM-BLS is an attractive alternative to SQUID-BLS for in-vivo measurement of LIC because it measures the same tissue property (i.e. magnetic susceptibility), while using a technology that is much more widely available (i.e. MRI).

Further, using the same gradient-echo acquisition as for QSM, R2* can also be estimated. Previous works have demonstrated the sensitivity of R2* to the presence of liver iron (20,21) and investigated its relationship to BLS (22,23). In work from Hernando et al., a confounder-corrected R2* technique was developed, which avoids the noise floor bias inherent to magnitude-based R2* mapping techniques while also properly accounting for the presence of fat in the liver (24,25).

Both techniques, i.e. QSM-BLS and confounder-corrected R2*, have demonstrated correlation to an MRI-based R2 relaxometry method for quantification of LIC (26) (Ferriscan®, Resonance Health, Claremont, Australia). However, R2-based methods are known to be confounded by factors other than iron concentration, including the rate of diffusion (27), which limits the accuracy of R2-based quantification of LIC. In contrast, magnetic susceptibility, as measured by SQUID-BLS, is directly related to the iron concentration, providing accurate measurement of LIC. Despite this advantage over R2-based methods, neither QSM-BLS nor confounder-corrected R2* has been compared to SQUID-BLS, in part because of the limited availability of a SQUID biomagnetometer.

In this work, we report results of the first study that performs QSM-BLS, confounder-corrected R2*, and SQUID-BLS in patients with liver iron overload. The goal of this study was to determine the relationships between QSM-BLS and confounder-corrected R2* to SQUID-BLS in patients with liver iron overload.

METHODS

Subjects

Twenty-two patients and two healthy controls were recruited at University Medical Center Hamburg-Eppendorf (Hamburg, Germany) for this prospective study. Patients were selected from a population that was undergoing MRI and SQUID-BLS as part of routine monitoring for iron overload (age: 14–73 yr, BMI: 15–30 kg/m^2, ferritin: 37–8216 μg/L). MRI and

SQUID-BLS were performed within one month of each other in 18 of 24 subjects, between one and two months in four subjects, and between two and four months in two subjects. Since patients were on an iron maintenance treatment, no significant difference of LIC was expected between MRI and SQUID experiments. For the 22 patients enrolled in this study, the diagnoses were: transfusion dependent thalassemia (n=11), Diamond-Blackfan anemia (n=4), sideroblastic anemia (n=3), compound hereditary hemochromatosis (n=1), myelodysplastic syndrome compounded by hereditary hemochromatosis (n=1), sickle cell disease (n=1), and osteomyelofibrosis (n=1). All subjects gave informed written consent for this study.

SQUID Susceptometry

The dual-channel SQUID-BLS system (Biomagnetic Technologies Inc., San Diego, USA) contains a sensor assembly with two symmetrical 2nd order gradiometer sensors coupled to radio frequency (RF)-SQUIDs aligned with superconducting magnetic field coils (1st order gradiometer with B_{max} = 20 mT), a water bellows coupling membrane (25 cm diameter) that serves as an infinite magnetic reference medium, a workstation for process control, and a low pass filtered data acquisition system with a data sampling rate of 1 kHz. Simultaneously acquired high pass filtered signals from locator loops (z-coil, two double D-coils) driven by AC currents (206 & 286 Hz) are used for distance measurements between the patient's skin and the lowest sensor coil and for horizontal positioning.

The SQUID-BLS system was calibrated using a water sphere and its known air-water magnetic volume susceptibility difference of $\Delta\chi_{air\text{-}water}$ = 9.396 ppm. Using a 1st order approximation, the susceptibility difference of the liver tissue ($\Delta\chi_{liver} = \chi_{liver}\text{-}\chi_{water}$) was fit to the voltage difference registered by the sensor assembly (28).

Patients underwent the following measurement procedure within a 30-minute scan time: in a tilted supine position, sonography was used to identify the liver, to determine optimal liver position and ellipsoidal organ geometry, and to measure skin-liver distance. After mounting a locator loop, the patient was positioned in the closest distance to the dewar tail of the SQUID. The subject was asked to hold his/her breath while the patient bed moved down at a rate of 0.7 cm/s followed by the water bellows. This vertical scan was repeated 3–5 times. The procedure is schematically illustrated in Figure 1, together with a sagittal ultrasound and a transverse MR image at the measurement position. With this patient positioning, the coverage of SQUID-BLS is concentrated to the anterior part of the right lobe of the liver, such that approximately 90% of the detected magnetic flux change originates from this portion of the liver (29).

Using the specific mass magnetic susceptibility for the hemosiderin/ferritin iron complex measured in human autopsy livers, $\xi_{Fe} = 1600 \cdot 10^{-9}$ m^3/kg_{Fe} (30,31), the in-vivo liver iron concentration was calculated as $LIC_{in\text{-}vivo} = \Delta\chi_{liver} / \xi_{Fe}$. Tabularized magnetic flux integrals for ellipsoidal liver and cylindrical thorax geometries, and assuming homogenously distributed $\Delta\chi_{liver}$, enabled real-time analysis of LIC (28).

After the patient was informed about the real-time result and released, a more complex offline analysis was performed (described later in *Data & Statistical Analyses*), which

accounts for magnetic objects (e.g. dental braces) and deviations caused by the thorax susceptibility.

MRI QSM and R2*

MR imaging was performed on a 3T clinical scanner (Ingenia, Philips Medical Systems, Best, The Netherlands) with a 28-channel torso array using a 3D six-echo, spoiled gradient-echo acquisition with bipolar readout. Acquisition parameters included: TE_1 = 1.2 ms, ΔTE = 1.0 ms, TR = 7.7 ms, flip angle = 3°, acquired resolution = 1.6 × 2.2 × 8 mm^3, matrix size = 256 × 144 × 32, parallel imaging acceleration factors = 1.9 (A/P) × 2.1 (L/R), and scan time approximately 19 s. Full 3D coverage of the liver was achieved within a single breath-hold.

Complex-valued, multi-echo images were reconstructed online from the acquired data using a phase-preserving SENSE-based approach (32). This processing resulted in a complex-valued 3D volume for each echo time (hereafter referred to as the ‘source images’).

The source images were processed offline using a chemical shift encoded (CSE) reconstruction (25,33,34), yielding estimates of the R2* map, B_0 field map, as well as separated water and fat images. The CSE reconstruction is a complex-based algorithm that avoids the noise floor bias inherent to magnitude-based R2* mapping techniques. In addition, this reconstruction models the spectral complexity of fat, which is also required to avoid bias in the estimate of R2*. A more comprehensive discussion of the confounder-corrected R2* mapping reconstruction is found in previously published works (24,25).

The estimated B_0 field map was processed using a QSM reconstruction that was developed for measuring susceptibility of the liver. This reconstruction performs a joint background field removal and dipole inversion to estimate the local susceptibility distribution. To regularize the ill-posed inversion, anatomical edge and fat constraints are incorporated into the parameter estimation (35,36). A more comprehensive presentation of the abdominal QSM reconstruction is found in previously published work (19).

Both the confounder-corrected R2* and the QSM reconstructions were implemented in Matlab (The Mathworks Inc., Natick, MA).

Data & Statistical Analyses

Offline SQUID-BLS analysis was performed using a 2^{nd} order approximation, which also took into account the magnetic contribution of the overlying thorax tissue (28). The measured voltage data points were fit to a model curve prescribed by the magnetic flux integrals of liver and thorax geometry and their respective magnetic susceptibilities (28). Any deviation from this curvature was suspected to originate from imperfect measurement quality, magnetic objects (dental braces, orthopedic implants, surgical staples, etc.), and especially, deviations from BMI-derived magnetic thorax susceptibility, which was established in previous work (37).

For the MRI experiment, a circular region of interest (ROI) with radius ~2 cm was placed in one central slice of the estimated susceptibility map. The ROI was placed in the right lobe of

the liver (away from major vessels and bile ducts), in a similar location as the region of coverage of SQUID-BLS. However, because SQUID-BLS cannot spatially localize the signal, exact co-localization to the SQUID-BLS measurement was not possible. Because QSM provides an estimate of relative susceptibility, an additional ROI was placed in the adjacent subcutaneous adipose tissue (SAT). The susceptibility in the liver was measured relative to the susceptibility in the SAT. The SAT was used as a reference point because it does not accumulate excess iron (38). The ROI in the liver was then copied to the R2* map. This ensured exact co-localization of susceptibility and R2* measurements in the liver.

From previous work, it is known that estimates of susceptibility and R2* are unreliable for patients with high LIC (25,39). In cases of high LIC, the transverse signal has decayed away before a sufficient number of measurements have been made. This leads to unreliable estimates of the R2* map and the B0 field map, which subsequently propagates to the susceptibility map estimate. Therefore, for subjects where the measured R2* > 800 s^{-1} (demonstrating high LIC), the data were excluded from statistical analyses. For the remaining data, linear regression analyses were performed in Excel (Microsoft, Redmond, WA) to assess the relationships between QSM-BLS and SQUID-BLS, liver R2* and SQUID-BLS, and the two MRI-based measures of liver iron overload.

RESULTS

Figure 2 shows R2* and susceptibility maps for one subject with normal LIC and another subject with moderate liver iron overload, using SQUID-BLS as the reference. Both R2* and QSM-BLS demonstrated sensitivity to the presence of iron in the liver. The estimates of liver R2* and liver susceptibility are also shown. As expected, the patient with liver iron overload exhibits both a higher R2* (increase of 561 s^{-1}) and a higher (i.e. less diamagnetic) magnetic susceptibility (increase of 1.59 ppm), which is expected since body iron stores are paramagnetic. Notice also the increased R2* and susceptibility in the spleen, which suggests excessive accumulation of iron in that organ as well.

In eight subjects, the measured R2* exceeded 800 s^{-1}, resulting in unreliable estimates of R2* and susceptibility. In one of these eight subjects, an extremely high LIC (34.2 mg Fe/g dry tissue as measured by SQUID-BLS) resulted in no measurable MR signal by the first echo of TE_1 = 1.2 ms. The data for the remaining subjects (two healthy subjects and 14 patients) were included in the statistical analyses.

Figure 3 shows the scatterplots of liver R2* versus SQUID-BLS and QSM-BLS versus SQUID-BLS. Figure 4 shows a scatter plot of QSM-BLS estimates versus R2* estimates. The results of the linear regression analyses are shown in Table 1.

DISCUSSION

In this study, we performed QSM-BLS, confounder-corrected R2*, and SQUID-BLS in subjects with varying degrees of liver iron overload. QSM-BLS measurements demonstrated a strong linear correlation to SQUID-BLS measurements (r^2 = 0.88). These findings are of clinical significance particularly because QSM-BLS measures the same quantitative property of tissue as SQUID-BLS, but using MRI, which has much greater availability than SQUID.

We determined the coefficient of determination between confounder-corrected R2* and SQUID-based susceptometry to be $r^2 = 0.88$. Gianesin et al. determined the relationship between R2* and magnetic iron detector susceptometry to be $r^2 = 0.68$ (23). There are many potential sources for this difference, including variations in MRI scanners and biomagnetometer systems. Further, unlike the method used by Gianesin et al., the R2* mapping technique used in this work avoided the confounding effects of noise floor bias and fat by fitting complex-valued data to a signal model that accounts for the presence of fat (25).

Linear regression analysis revealed a discrepancy (slope = 0.49) in the magnetic susceptibility estimates between QSM-BLS and SQUID-BLS. Similar discrepancies have been noted in brain QSM as demonstrated by Wang and Liu (10). In their review, an assessment of the accuracy of various QSM techniques using simulated brain data found slopes ranging from 0.63–0.99. In general, the cause of these discrepancies is still unknown. However, recent works have demonstrated the effects of spatial resolution, including a large slice thickness, on the accuracy of QSM (40,41). In this current study, the data were acquired using a relatively large slice thickness of 8 mm, which was required to achieve full 3D coverage of the liver in one breath-hold. Therefore, it is conceivable that the large slice thickness contributed to the bias that was observed in this study. Despite this current discrepancy, the strong correlation between QSM-BLS and SQUID-BLS suggests the promise of QSM-BLS for assessment of liver iron overload.

Both SQUID-BLS and QSM-BLS aim to measure liver susceptibility, in order to quantify liver iron concentration. Despite this similar goal, there are significant differences in the methodology used to derive liver susceptibility values. SQUID-BLS is a planar method that uses electronic magnetometers that are sensitive to nearby magnetized tissues. The measurement from SQUID-BLS is assumed to represent the magnetic susceptibility throughout the entire liver. In contrast, QSM-BLS is able to localize the signal, and thus provides 3D spatial maps of the susceptibility distribution. Further, SQUID-BLS has greater dynamic range than QSM-BLS (and confounder-corrected R2*), which must acquire a sufficient number of measurements before the transverse signal has decayed away. Thus, while SQUID-BLS was sensitive to the full range of LIC for subjects in this study, QSM-BLS was not. In particular, for eight subjects in this study, high LIC caused low SNR in the liver, which resulted in unreliable estimates of liver susceptibility and R2*. Improvements to the data acquisition and parameter mapping of these MRI-based techniques will be necessary to match the dynamic range that is currently available using SQUID-BLS.

Similar to previous work (19), this study demonstrated a strong correlation between QSM-BLS and R2*. This correlation is not surprising since both susceptibility and R2* are sensitive to the presence of iron. However, this finding raises the question as to whether there are any differences between these two MRI-based techniques for assessing liver iron overload. That is, can these two techniques be used interchangeably, or do they provide complementary information regarding liver iron overload? Further technical development of QSM for liver iron overload is required before the relationship between susceptibility and R2* can be fully elucidated. It must also be noted that both parameters can be estimated from the same multi-gradient-echo acquisition, as was done in this study.

In conclusion, we have investigated the relationships between QSM-BLS, confounder-corrected R2*, and SQUID-BLS in subjects with liver iron overload. Both MRI-based estimates were strongly correlated with SQUID-BLS. The results of this study further demonstrate the feasibility for QSM-BLS and confounder-corrected R2* to assess liver iron overload. Further, similar to SQUID-BLS, QSM-BLS has the potential to quantify LIC by measuring a quantitative tissue property (i.e. magnetic susceptibility) that has a direct and known relationship to iron concentration.

Acknowledgments

We gratefully acknowledge the support of Rosemarie Kongi (University Medical Center Hamburg-Eppendorf) for operating the SQUID biomagnetometer and for coordinating the patients for MRI. We also appreciate the constructive feedback provided by Marcela Weyhmiller, Ph.D. (UCSF Benioff Children's Hospital and Research Center).

This work was supported by the NIH (R01DK083380, R01DK088925, R01DK100651, K24DK102595, and UL1TR00427). We also acknowledge GE Healthcare and Bracco Diagnostics who provide research support to the University of Wisconsin-Madison.

References

1. Frazer DM, Anderson GJ. Iron imports. I. Intestinal iron absorption and its regulation. American Journal of Physiology-Gastrointestinal and Liver Physiology. 2005; 289(4):G631–G635. [PubMed: 16160078]
2. Porter JB. Practical management of iron overload. British Journal of Haematology. 2001; 115(2): 239–252. [PubMed: 11703317]
3. Vichinsky E. Oral iron chelators and the treatment of iron overload in pediatric patients with chronic anemia. Pediatrics. 2008; 121(6):1253–1256. [PubMed: 18519495]
4. Nielsen P, Günther U, Dürken M, Fischer R, Düllmann J. Serum ferritin iron in iron overload and liver damage: correlation to body iron stores and diagnostic relevance. Journal of Laboratory and Clinical Medicine. 2000; 135(5):413–418. [PubMed: 10811057]
5. Brittenham GM, Badman DG. Noninvasive measurement of iron: report of an NIDDK workshop. Blood. 2003; 101(1):15–19. [PubMed: 12393526]
6. Emond MJ, Bronner MP, Carlson TH, Lin M, Labbe RF, Kowdley KV. Quantitative study of the variability of hepatic iron concentrations. Clinical Chemistry. 1999; 45(3):340–346. [PubMed: 10053034]
7. Brittenham GM, Farrell DE, Harris JW, Feldman ES, Danish EH, Muir WA, Tripp JH, Bellon EM. Magnetic-susceptibility measurement of human iron stores. New England Journal of Medicine. 1982; 307(27):1671–1675. [PubMed: 7144866]
8. Paulson D, Fagaly R, Toussaint R, Fischer R. Biomagnetic susceptometer with SQUID instrumentation. IEEE Transactions on Magnetics. 1991; 27(2):3249–3252.
9. Marinelli M, Cuneo S, Gianesin B, Lavagetto A, Lamagna M, Oliveri E, Sobrero G, Terenzani L, Forni GL. Non-invasive measurement of iron overload in the human body. IEEE Transactions on Applied Superconductivity. 2006; 16(2):1513–1518.
10. Wang Y, Liu T. Quantitative susceptibility mapping (QSM): decoding MRI data for a tissue magnetic biomarker. Magnetic Resonance in Medicine. 2015; 73(1):82–101. [PubMed: 25044035]
11. Liu C, Wei H, Gong N-J, Cronin M, Dibb R, Decker K. Quantitative Susceptibility Mapping: Contrast Mechanisms and Clinical Applications. Tomography. 2015; 1(1):3–17. [PubMed: 26844301]
12. Haacke EM, Liu S, Buch S, Zheng W, Wu D, Ye Y. Quantitative susceptibility mapping: current status and future directions. Magnetic Resonance Imaging. 2015; 33(1):1–25. [PubMed: 25267705]

13. Schweser F, Deistung A, Lehr BW, Reichenbach JR. Differentiation between diamagnetic and paramagnetic cerebral lesions based on magnetic susceptibility mapping. Medical Physics. 2010; 37(10):5165–5178. [PubMed: 21089750]
14. Chen W, Zhu W, Kovanlikaya I, Kovanlikaya A, Liu T, Wang S, Salustri C, Wang Y. Intracranial calcifications and hemorrhages: characterization with quantitative susceptibility mapping. Radiology. 2014; 270(2):496–505. [PubMed: 24126366]
15. Langkammer C, Schweser F, Krebs N, Deistung A, Goessler W, Scheurer E, Sommer K, Reishofer G, Yen K, Fazekas F, Ropele S, Reichenbach JR. Quantitative susceptibility mapping (QSM) as a means to measure brain iron? A post mortem validation study. Neuroimage. 2012; 62(3):1593–1599. [PubMed: 22634862]
16. Bilgic B, Pfefferbaum A, Rohlfing T, Sullivan EV, Adalsteinsson E. MRI estimates of brain iron concentration in normal aging using quantitative susceptibility mapping. Neuroimage. 2012; 59(3): 2625–2635. [PubMed: 21925274]
17. Bonekamp D, Barker PB, Leigh R, van Zijl PCM, Li X. Susceptibility-based analysis of dynamic gadolinium bolus perfusion MRI. Magnetic Resonance in Medicine. 2015; 73(2):544–554. [PubMed: 24604343]
18. Xu B, Spincemaille P, Liu T, Prince MR, Dutruel S, Gupta A, Thimmappa ND, Wang Y. Quantification of cerebral perfusion using dynamic quantitative susceptibility mapping. Magnetic Resonance in Medicine. 2015; 73(4):1540–1548. [PubMed: 24733457]
19. Sharma SD, Hernando D, Horng DE, Reeder SB. Quantitative susceptibility mapping in the abdomen as an imaging biomarker of hepatic iron overload. Magnetic Resonance in Medicine. 2015; 74(3):673–683. [PubMed: 25199788]
20. Wood JC, Enriquez C, Ghugre N, Tyzka JM, Carson S, Nelson MD, Coates TD. MRI R2 and R2* mapping accurately estimates hepatic iron concentration in transfusion-dependent thalassemia and sickle cell disease patients. Blood. 2005; 106(4):1460–1465. [PubMed: 15860670]
21. Hankins JS, McCarville MB, Loeffler RB, Smeltzer MP, Onciu M, Hoffer FA, Li C-S, Wang WC, Ware RE, Hillenbrand CM. R2* magnetic resonance imaging of the liver in patients with iron overload. Blood. 2009; 113(20):4853–4855. [PubMed: 19264677]
22. Carneiro AAO, Fernandes JP, de Araujo DB, Elias J, Martinelli AL, Covas DT, Zago MA, Angulo IL, St Pierre T, Baffa O. Liver iron concentration evaluated by two magnetic methods: magnetic resonance imaging and magnetic susceptometry. Magnetic Resonance in Medicine. 2005; 54(1): 122–128. [PubMed: 15968652]
23. Gianesin B, Zefiro D, Musso M, Rosa A, Bruzzone C, Balocco M, Carrara P, Bacigalupo L, Banderali S, Rollandi G, Gambaro M, Marinelli M, Forni G. Measurement of liver iron overload: Noninvasive calibration of MRI-R2* by magnetic iron detector susceptometer. Magnetic Resonance in Medicine. 2012; 67(6):1782–1786. [PubMed: 22135193]
24. Hernando D, Vigen KK, Shimakawa A, Reeder SB. R2* mapping in the presence of macroscopic B0 field variations. Magnetic Resonance in Medicine. 2012; 68(3):830–840. [PubMed: 22161866]
25. Hernando D, Kramer JH, Reeder SB. Multipeak fat-corrected complex R2* relaxometry: Theory, optimization, and clinical validation. Magnetic Resonance in Medicine. 2013; 70(5):1319–1331. [PubMed: 23359327]
26. Pierre TGS, Clark PR, Chua-anusorn W, Fleming AJ, Jeffrey GP, Olynyk JK, Pootrakul P, Robins E, Lindeman R. Noninvasive measurement and imaging of liver iron concentrations using proton magnetic resonance. Blood. 2005; 105(2):855–861. [PubMed: 15256427]
27. Ghugre NR, Wood JC. Relaxivity-iron calibration in hepatic iron overload: Probing underlying biophysical mechanisms using a Monte Carlo model. Magnetic Resonance in Medicine. 2011; 65(3):837–847. [PubMed: 21337413]
28. Fischer, R., Farrell, D. Magnetism in Medicine: A Handbook. 2. 2007. Liver iron susceptometry; p. 529-549.
29. Fischer, R. Magnetism in Medicine: A Handbook. 1. 1998. Liver iron susceptometry; p. 286-301.
30. Bauman JH, Harris JW. Estimation of hepatic iron stores by vivo measurement of magnetic susceptibility. The Journal of Laboratory and Clinical Medicine. 1967; 70(2):246. [PubMed: 6029057]
31. Shoden A, Sturgeon P. Hemosiderin. Acta Haematologica. 1960; 23(6):376–392.

32. Pruessmann KP, Weiger M, Scheidegger MB, Boesiger P. SENSE: sensitivity encoding for fast MRI. Magnetic Resonance in Medicine. 1999; 42(5):952–962. [PubMed: 10542355]
33. Dixon WT. Simple proton spectroscopic imaging. Radiology. 1984; 153(1):189–194. [PubMed: 6089263]
34. Reeder SB, Wen Z, Yu H, Pineda AR, Gold GE, Markl M, Pelc NJ. Multicoil Dixon chemical species separation with an iterative least-squares estimation method. Magnetic Resonance in Medicine. 2004; 51(1):35–45. [PubMed: 14705043]
35. de Rochefort L, Liu T, Kressler B, Liu J, Spincemaille P, Lebon V, Wu J, Wang Y. Quantitative susceptibility map reconstruction from MR phase data using bayesian regularization: validation and application to brain imaging. Magnetic Resonance in Medicine. 2010; 63(1):194–206. [PubMed: 19953507]
36. Liu T, Liu J, de Rochefort L, Spincemaille P, Khalidov I, Ledoux JR, Wang Y. Morphology enabled dipole inversion (MEDI) from a single-angle acquisition: Comparison with COSMOS in human brain imaging. Magnetic Resonance in Medicine. 2011; 66(3):777–783. [PubMed: 21465541]
37. Fischer, R., Engelhardt, R., Nielsen, P. The influence of thorax tissue in biomagnetic liver susceptometry (BLS). Proceedings of the 13th International Conference on Biomagnetism; 2002; Jena, Germany. p. 1063-1065.
38. Knutson M, Wessling-Resnick M. Iron metabolism in the reticuloendothelial system. Critical Reviews in Biochemistry and Molecular Biology. 2003; 38(1):61–88. [PubMed: 12641343]
39. Sharma, SD., Hernando, D., Horng, DE., Reeder, SB. Optimizing the data acquisition strategy for quantitative susceptibility mapping in the liver. Proceedings of the 23rd Annual Meeting of the ISMRM; 2015; Toronto, Canada. p. 1713
40. Zhou, D., Liu, T., Zhang, J., Wang, Y. Accuracy of the QSM reconstruction: dependence on imaging resolution and B0 strength. 3rd QSM Workshop on Phase Contrast and Quantitative Susceptibility Mapping; 2014; Durham, USA. p. 94
41. Karsa, A., Biondetti, E., Punwani, S., Shmueli, K. The effect of large slice thickness and spacing and low coverage on the accuracy of susceptibility mapping. Proceedings of the 24th Annual Meeting of the ISMRM; 2016; Singapore. p. 1555

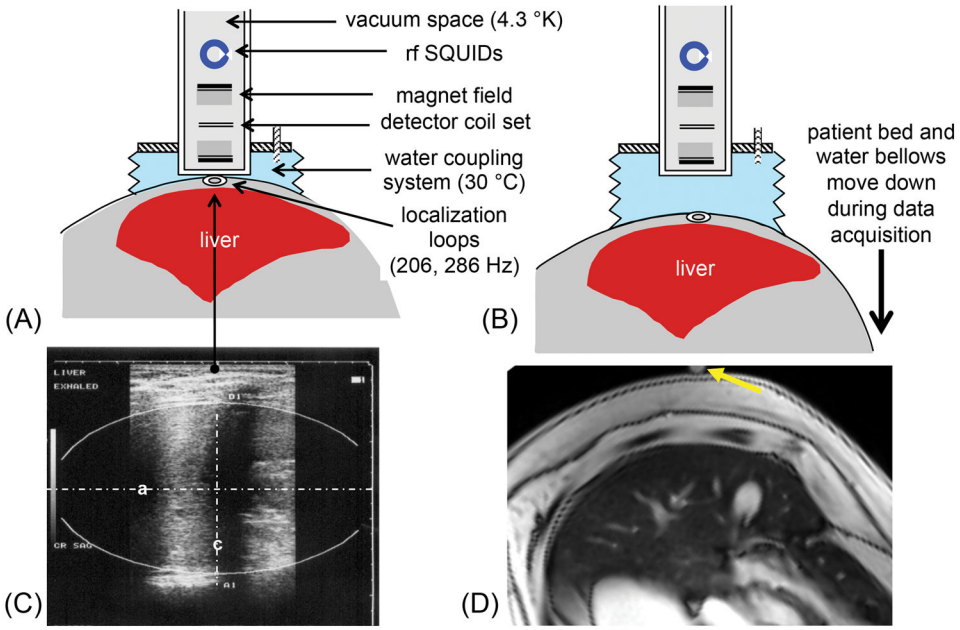

Figure 1.

Schematic illustration of the liver iron measurement with a SQUID biomagnetometer system. (A) Starting position of liver and SQUID system. (B) The patient and water coupling system move down during the data acquisition (over a 13 second time window). The vertical scan is repeated 3–5 times. (C) Ultrasound imaging is used to measure the skin-liver distance and the ellipsoidal organ geometry. (D) A rotated axial MR image aligned with the SQUID-BLS position is shown. The yellow arrow marks the measurement position for SQUID-BLS.

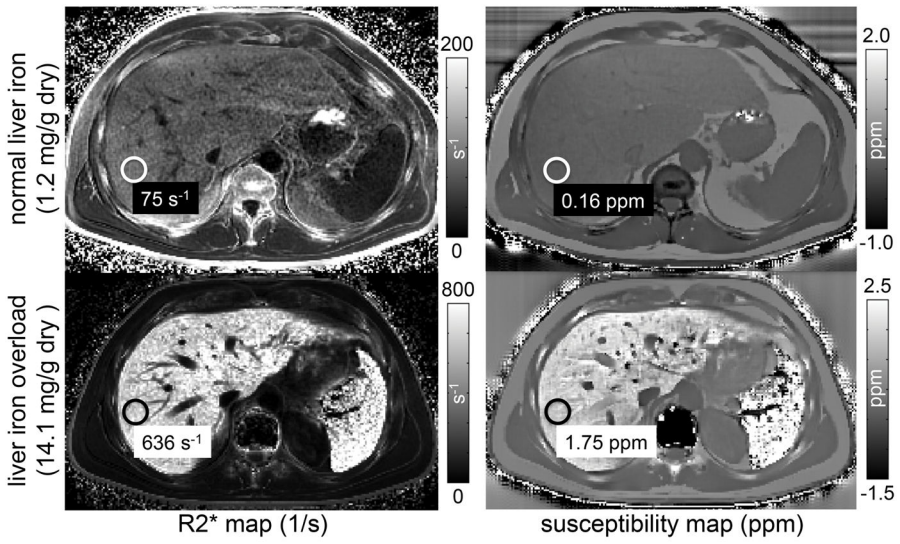

Figure 2.

Both MRI-based R2* mapping and QSM are sensitive to the presence of iron in the liver. The figure shows R2* maps (left) and susceptibility maps (right) estimated from a subject with normal liver iron (top) and with liver iron overload (bottom). SQUID-BLS estimates of LIC are reported. The susceptibility measurements reflect the change in liver susceptibility due to the presence of iron. For the subject with liver iron overload, notice the increase in R2* and susceptibility in the spleen, suggesting the presence of iron overload in that organ as well.

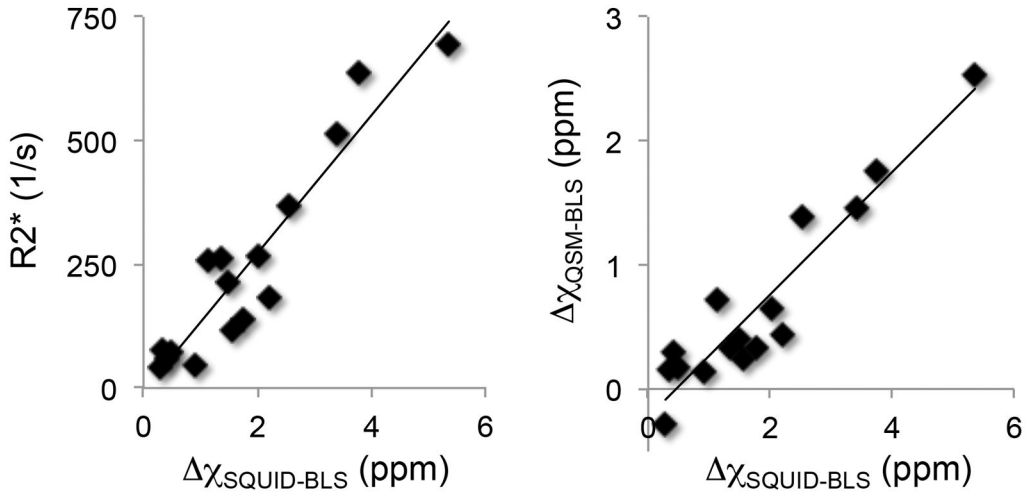

Figure 3.

Scatterplots of R2* versus SQUID-BLS (left) and QSM-BLS versus SQUID-BLS (right) demonstrate strong correlations between both MRI-based measures of liver iron and SQUID-BLS. The coefficient of determination between R2* and SQUID-BLS was $r^2 = 0.88$. Linear regression between the two BLS methods demonstrated the following relationship: QSM-BLS = (−0.22 ± 0.11) + (0.49 ± 0.05) · SQUID-BLS, with $r^2 = 0.88$.

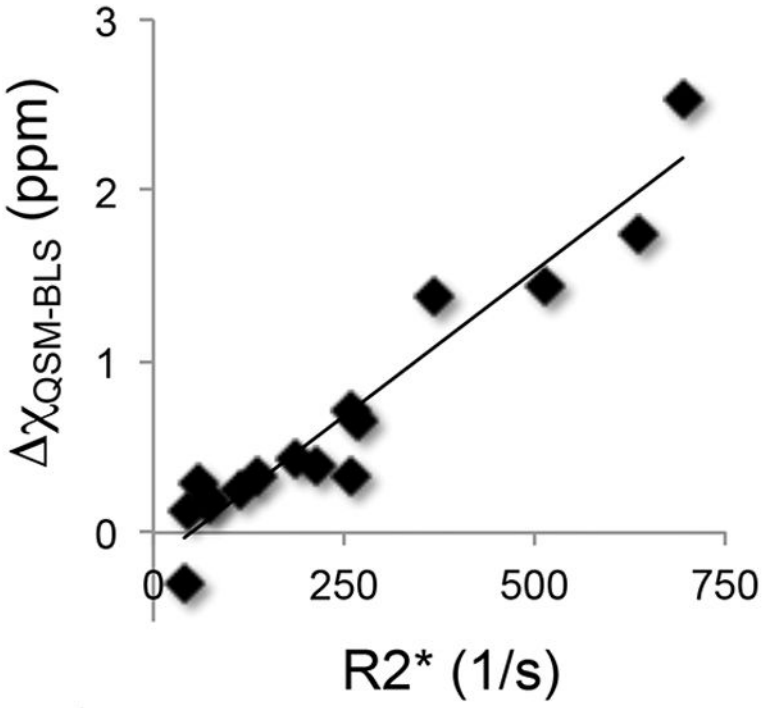

Figure 4.

QSM-BLS demonstrates strong correlation to R2*. The linear regression analysis between these two MR-based measures of LIC yielded: QSM-BLS = (−0.17 ± 0.09) + (0.0034 ± 0.0003) · R2*, with $r^2 = 0.92$.

Table 1

Linear regression analyses comparing QSM-BLS, R2* mapping, and SQUID-BLS in two healthy controls and 14 patients with liver iron overload show strong correlations between each pair of measurements.

	slope	intercept	r^2
QSM-BLS vs. SQUID-BLS	0.49 ± 0.05	−0.22 ± 0.11 ppm	0.88
R2* vs. SQUID-BLS	139.47 ± 13.59 s^{-1}/ppm	−6.29 ± 30.76 s^{-1}	0.88
QSM-BLS vs. R2*	0.0034 ± 0.0003 ppm/s^{-1}	−0.17 ± 0.09 ppm	0.92